Journal of Zhejiang University-SCIENCE A (Applied Physics & Engineering)
ISSN 1673-565X (Print); ISSN 1862-1775 (Online)
www.zju.edu.cn/jzus; www.springerlink.com
E-mail: jzus@zju.edu.cn

Dynamic responses of cable-stayed bridges to vehicular loading including the effects of the local vibration of cables*

He ZHANG, Xu XIE†‡

(*Department of Civil Engineering, Zhejiang University, Hangzhou 310058, China*)

†E-mail: xiexu@zju.edu.cn

Received July 27, 2010; Revision accepted Mar. 9, 2011; Crosschecked July 11, 2011

Abstract: Stay cables, the primary load carrying components of cable-stayed bridges (CSBs), are characterised by high flexibility which increases with the span of the bridge. This makes stay cables vulnerable to local vibrations which may have significant effects on the dynamic responses of long-span CSBs. Hence, it is essential to account for these effects in the assessment of the dynamics CSBs. In this paper, the dynamic responses of CSBs under vehicular loads are studied using the finite element method (FEM), while the local vibration of stay cables is analyzed using the substructure method. A case study of a cable-stayed steel bridge with a center span of 448 m demonstrates that stay cables undergo large displacements in the primary mode of the whole bridge although, in general, a cable's local vibrations are not obvious. The road surface roughness has significant effects on the interaction force between the deck and vehicle but little effect on the global response of the bridge. Load impact factors of the main girder and tower are small, and the impact factors of the tension of cables are larger than those of the displacements of girders and towers.

Key words: Cable-stayed bridge (CSB), Vehicular load, Local vibration of cable, Impact effect
doi:10.1631/jzus.A1000351 **Document code:** A **CLC number:** U448.27

1 Introduction

The cable-stayed bridge (CSB), a kind of long-period 3D structure, has experienced a dramatic increase both in number and in the length of the center/effective span during the past two decades. The design of a CSB is based primarily on its stiffness, state of stresses, and stability under live loads. The impact effect, which is the ratio of the dynamic displacement response to the static deformation due to vehicles, significantly affects the reliability of CSBs and related economic aspects. Stay cables are the main load-carrying members in CSBs and are apt to vibrate because of their light weight, very low stiffness and structural damping when subjected to external stimulation, such as wind, rain, earthquake, or traffic load. Intensive vibration tends to lead to fatigue damage in cables and around the anchorage joint between the cable and the suspending deck or tower. Hence, in the dynamics assessment of CSBs under vehicular loads, it is very important to account for the effects of the vibration of stay cables on the dynamic responses of girders, towers, and the whole bridge (Abdel-Ghaffar and Khalifa, 1991; Caetano *et al.*, 2000).

Many investigators have reported the analysis of dynamic responses of CSBs due to vehicular loads. Zaman *et al.* (1996) proposed a structural impedance algorithm for the dynamic responses of CSBs due to moving vehicles. Cable-stayed bridge-vehicle interaction was analyzed by Guo and Xu (2001) who idealized each heavy road vehicle as 13 rigid bodies connected by springs and dampers. In their analysis,

‡ Corresponding author

* Project (No. 20100481432) supported by the China Postdoctoral Science Foundation

the road surface roughness was taken into consideration and described as a realization of a random process featured as a power spectral density (PSD) function. Au *et al.* (2001) investigated the effects of random road surface roughness on the impact factor of cable-stayed concrete bridges using a zero-mean stationary Gaussian random process. They found that the effect of road surface roughness on stay cables depends on the cable length. The shorter is the cable, the more significant is the impact effect, and the effect on the longest cables may even be negligible. Das *et al.* (2004) also studied the effects of random road surface roughness on the impact effects of a three-span CSB. They examined the errors due to discretizations in space and time domains to ensure an accurate assessment of the impact factor of the bridge. A 3D numerical model, taking into account the bridge-vehicle dynamic interaction, was developed by Calcada *et al.* (2005b) to investigate the dynamic responses of a real CSB. Input parameters, including the number and lay-out of moving vehicles, passing speed, and the spatially varying road surface roughness, were obtained directly from field tests (Calcada *et al.*, 2005a). The dynamic amplification factors over the static responses were comprehensively investigated by accounting for the road surface roughness, vehicle features and traffic flow, which were finally verified by experimental results (Calcada *et al.*, 2005a). Recently, the dynamic impact effects moving loads on long-span CSBs were analyzed by Bruno *et al.* (2008) using a continuum model in which the interaction forces between different structural components were described by means of continuous distributed functions. Stay cables were modeled using a truss element, accounting for the sag effect by using the secant Dischinger modulus. Au *et al.* (2009) made a good simulation of the vibration due to moving loads of the Ting-Kau Bridge in Hong Kong, based on a one-year-measurement of vehicular loads, which made the dynamic analysis of CSBs more realistic.

These studies have provided a comprehensive investigation of bridge-vehicle dynamic interactions and the impact effects of vehicular loads on CSBs. However, they did not consider the effects of the vibration of stay cables. For a long-span CSB, because of its flexibility, some of the natural frequencies of the bridge deck become very low and fall into the range of the frequencies of cables with different lengths, which creates the possibility of resonance between the global vibration of the bridge and local vibrations of the cables. To investigate the mechanism of interaction between the "local" and "global" vibrations of the cable-beam system, a nonlinear analytical model was proposed by Fujino *et al.* (1993). Later, they studied the problem in a more general manner (Warnitchai *et al.*, 1995), treating the effect of the cable support on the beam as quasi-static motions and expressing the vibration of the cable as a combination of the quasi-static motions of the cable supports and the modal motions of the cable. The cable-beam system was also used by Gattulli and Lepidi (2007) to investigate the localization and veering phenomena of the dynamic characteristics of the system. Caetano (2008) analyzed the dynamic responses of a CSB to moving loads and considered the interaction between the cables and the deck. Wu *et al.* (2003) studied the response characteristics of local vibrations in stay cables on an existing CSB with a span of 350 m. A single degree of freedom (DOF) vehicular model was adopted in their research and the superposition method was used to obtain the dynamic responses of the bridge. They found that small deformation vibrations in cables will occur when the bridge is subjected to traffic loading. Considering the complexity of the characteristics of CSBs and the principles of the superposition method, the precision of the calculation will depend on the selection of the modes included in the model.

In this paper, the finite element method (FEM) is used to investigate the dynamic response of a bridge under vehicular loads, and the effect of a cable's local vibration is considered using a substructure method. Here, the road surface roughness is considered using the Monte Carlo method, and a 4-DOF lumped mass model is adopted for the vehicle. The coupling vibration between the bridge and a vehicle is calculated using the Newmark-β method of direct integration. A CSB with a center span of 448 m is considered in this case study. Cable-deck coupling vibrations due to vehicles traveling with different velocities are investigated. The impact factors for various structural components and physical quantities are calculated and discussed. This case study offers a theoretical reference for analysis of a cable's vibration and the determination of the impact effect of CSBs.

2 Numerical model of the coupling system of a bridge and vehicle

2.1 Equations of motion for the bridge

The vibration of CSBs due to vehicular loading was analyzed via FEM with beam and cable elements. The substructure method proposed by Nagai *et al.* (1993) was applied to consider the local vibration of cables. Each simulated cable was divided into $n-1$ interlinking truss elements (Fig. 1).

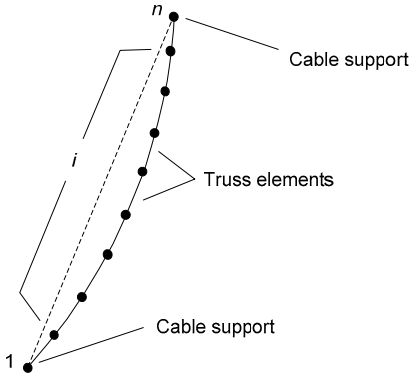

Fig. 1 FEM model of the cable

To improve the computational efficiency of the dynamic analysis of CSBs, the local vibrations of cables were considered using a substructure method. According to the method of superposition, the vibrations of the cable are composed of vibrations of cable supports and several modes. The accuracy of the method depends on the quantity of modes adopted in calculation. For flexible structures such as cables, the vibration is composed primarily of the components of low orders of modes.

The equation of motion of the free vibrations of each cable can be expressed as

$$\begin{bmatrix} \boldsymbol{m}_{11} & \boldsymbol{m}_{1i} & \boldsymbol{0} \\ \boldsymbol{m}_{i1} & \boldsymbol{m}_{ii} & \boldsymbol{m}_{in} \\ \boldsymbol{0} & \boldsymbol{m}_{ni} & \boldsymbol{m}_{nn} \end{bmatrix} \begin{bmatrix} \ddot{\boldsymbol{d}}_1 \\ \ddot{\boldsymbol{d}}_i \\ \ddot{\boldsymbol{d}}_n \end{bmatrix} + \begin{bmatrix} \boldsymbol{k}_{11} & \boldsymbol{k}_{1i} & \boldsymbol{0} \\ \boldsymbol{k}_{i1} & \boldsymbol{k}_{ii} & \boldsymbol{k}_{in} \\ \boldsymbol{0} & \boldsymbol{k}_{ni} & \boldsymbol{k}_{nn} \end{bmatrix} \begin{bmatrix} \boldsymbol{d}_1 \\ \boldsymbol{d}_i \\ \boldsymbol{d}_n \end{bmatrix} = \begin{bmatrix} \boldsymbol{0} \\ \boldsymbol{0} \\ \boldsymbol{0} \end{bmatrix}, \quad (1)$$

where $\boldsymbol{m}_{ij}$ are the sub-matrices of the mass matrix, $\boldsymbol{k}_{ij}$ are the sub-matrices of the stiffness matrix, $\boldsymbol{d}_1$, $\boldsymbol{d}_n$ are the displacement vectors at cable supports and $\boldsymbol{d}_i$ represents the displacement vector of the inner nodes of the cable. According to the superposition method (Fig. 2), $\boldsymbol{d}_i$ can be separated into two parts, the movement of cable supports and modal motions. In this study, the modal motion of a cable is assumed to be a combination of several lower-order modes of the cable with fixed supports. Thus, $\boldsymbol{d}_i$ is approximated as

$$\boldsymbol{d}_i \approx \boldsymbol{T}_1\boldsymbol{d}_1 + \boldsymbol{T}_2\boldsymbol{d}_n + \boldsymbol{\Phi}\boldsymbol{q}, \quad (2)$$

where

$$\begin{cases} \boldsymbol{T}_1 = -\boldsymbol{k}_{ii}^{-1}\boldsymbol{k}_{i1}, \\ \boldsymbol{T}_2 = -\boldsymbol{k}_{ii}^{-1}\boldsymbol{k}_{in}, \end{cases} \quad (3)$$

and $\boldsymbol{q}$ is the generalized coordinates vector. $\boldsymbol{\Phi}$ is the modal matrix of a cable with two fixed ends, and is obtained by solving the eigenvalue problem from Eq. (1),

$$\boldsymbol{\Phi} = \begin{bmatrix} \boldsymbol{\varphi}_1 & \boldsymbol{\varphi}_2 & \cdots & \boldsymbol{\varphi}_m \end{bmatrix}, \quad (4)$$

where $\boldsymbol{\varphi}_i$ is the ith natural mode and m is the quantity of modes adopted in the vibration calculation.

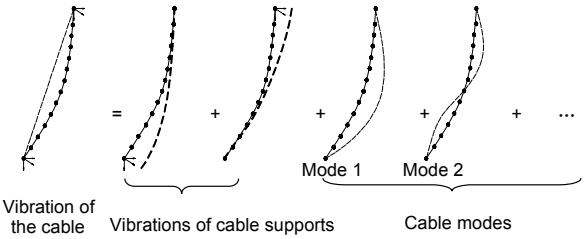

Fig. 2 Method for calculating the local vibration of cables

Hence, Eq. (1) can be transformed into Eq. (5) as

$$\tilde{\boldsymbol{M}}_{\mathrm{c}} \begin{bmatrix} \ddot{\boldsymbol{d}}_1 \\ \ddot{\boldsymbol{d}}_n \\ \ddot{\boldsymbol{q}} \end{bmatrix} + \tilde{\boldsymbol{K}}_{\mathrm{c}} \begin{bmatrix} \boldsymbol{d}_1 \\ \boldsymbol{d}_n \\ \boldsymbol{q} \end{bmatrix} = \boldsymbol{0}, \quad (5)$$

where

$$\begin{cases} \tilde{\boldsymbol{M}}_{\mathrm{c}} = \boldsymbol{T}_{\mathrm{s}}^{\mathrm{T}}\boldsymbol{M}_{\mathrm{c}}\boldsymbol{T}_{\mathrm{s}}, \\ \tilde{\boldsymbol{K}}_{\mathrm{c}} = \boldsymbol{T}_{\mathrm{s}}^{\mathrm{T}}\boldsymbol{K}_{\mathrm{c}}\boldsymbol{T}_{\mathrm{s}}, \end{cases} \quad (6)$$

where $\boldsymbol{M}_{\mathrm{c}}$ and $\boldsymbol{K}_{\mathrm{c}}$ are the mass and stiffness matrices, respectively, $\tilde{\boldsymbol{M}}_{\mathrm{c}}$ and $\tilde{\boldsymbol{K}}_{\mathrm{c}}$ are the equivalent mass and stiffness matrices, respectively after freedom quantity reduction, and

$$\boldsymbol{T}_{\mathrm{s}} = \begin{bmatrix} \boldsymbol{I} & \boldsymbol{0} & \boldsymbol{0} \\ \boldsymbol{T}_1 & \boldsymbol{T}_2 & \boldsymbol{\Phi} \\ \boldsymbol{0} & \boldsymbol{I} & \boldsymbol{0} \end{bmatrix}, \quad (7)$$

where $\boldsymbol{I}$ is the unit matrix.

Girders and towers are simulated with 3D beam elements. The cross-section of a main girder is depicted in Fig. 3, and is composed of the girder and the accessory members such as the pavement and railings, whose stiffnesses are not considered. G and S denote the geometry center and the shear center, respectively. The assumption that the cross-sections remain plane and normal to the neutral axis holds when deformation of the girder occurs. The displacements of the cross-section can be expressed as

$$\begin{cases} W(x,y,z) = w_{\mathrm{G}} - xu_{\mathrm{s}}' - yv_{\mathrm{s}}', \\ U(x,y,z) = u_{\mathrm{s}} - (y - y_{\mathrm{s}})\theta_z, \\ V(x,y,z) = v_{\mathrm{s}} + x\theta_z, \end{cases} \tag{8}$$

where W, U and V are the axial, lateral and vertical displacements, respectively, of corresponding points in the cross-section, w_{G} is the axial displacement of the geometry center, u_{s} and v_{s} are the lateral displacements of the shearing center, and θ_z is the torsion angle. Other parameters are shown in Fig. 3. x-, y- and z-axis are set in the lateral, vertical and longitudinal directions respectively, of the bridge. u_{s}' and v_{s}' are the differentials of u_{s} and v_{s} respectively, about the z-axis.

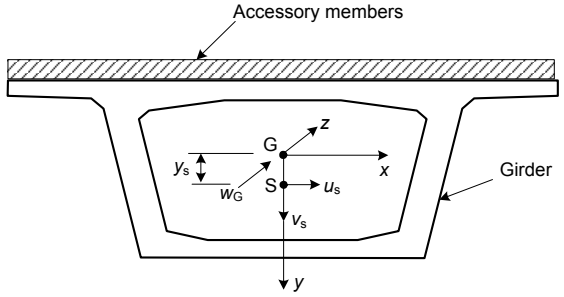

Fig. 3 Cross-section of box girder

Taking account of the differences in density between the girder and the accessory members, the kinetic energy T_{e} can be expressed as

$$T_{\mathrm{e}} = \frac{\gamma_{\mathrm{s}}}{2g}\left\{\int_{V_{\mathrm{s}}}\left(\dot{U}^2 + \dot{V}^2 + \dot{W}^2\right)\mathrm{d}V + \frac{\gamma_1}{\gamma_{\mathrm{s}}}\int_{V_1}\left(\dot{U}^2 + \dot{V}^2 + \dot{W}^2\right)\mathrm{d}V\right\}, \tag{9}$$

where a dot above the variable indicates the derivative with respect to time t, and g is the acceleration due to gravity. γ_{s} and γ_1 are the weights of unit volume, and V_{s} and V_1 are the volumes of the girder and the accessory members, respectively.

Neglecting the shear strain caused by shear force, the strain energy U_{e} of the beam element is

$$U_{\mathrm{e}} = \frac{1}{2}\int_{V_{\mathrm{s}}}(E\varepsilon_z^2 + G\gamma^2)\mathrm{d}V_{\mathrm{s}}, \tag{10}$$

where E is Young's modulus, G is the shear modulus, ε_z is the longitudinal strain, and γ is the torsional shear strain.

The potential energy of the element due to external force can be expressed as

$$P_{\mathrm{e}} = \int_z \left\{p_x u_{\mathrm{s}} + p_y v_{\mathrm{s}} + p_z w_{\mathrm{G}} + m_{\mathrm{t}}\theta_z\right\}\mathrm{d}z, \tag{11}$$

where p_x, p_y and p_z are the distributed loads in the x-, y-, and z-direction, respectively, and m_{t} is the distributed torsion moment.

By introducing the kinetic energy, the strain energy, and the potential energy due to external force into the Hamilton principle, the equation of motion of a 3D beam element can be expressed as

$$\begin{cases} EAw_{\mathrm{G}}'' - \dfrac{\gamma_{\mathrm{s}}}{g}A_{\mathrm{eq}}\ddot{w}_{\mathrm{G}} = -p_z, \\ EI_y u_{\mathrm{s}}^{(4)} + \dfrac{\gamma_{\mathrm{s}}}{g}A_{\mathrm{eq}}\ddot{u}_{\mathrm{s}} + \dfrac{\gamma_{\mathrm{s}}}{g}H_u\ddot{\theta}_z = p_x, \\ EI_x v_{\mathrm{s}}^{(4)} + \dfrac{\gamma_{\mathrm{s}}}{g}A_{\mathrm{eq}}\ddot{v}_{\mathrm{s}} - \dfrac{\gamma_{\mathrm{s}}}{g}H_v\ddot{\theta} = p_y, \\ GJ\theta_z'' + \dfrac{\gamma_{\mathrm{s}}}{g}H_u\ddot{u}_{\mathrm{s}} - \dfrac{\gamma_{\mathrm{s}}}{g}H_v\ddot{v}_{\mathrm{s}} + \dfrac{\gamma_{\mathrm{s}}}{g}I_p\ddot{\theta}_z = p_x y_{\mathrm{s}} + m_{\mathrm{t}}, \end{cases} \tag{12}$$

where A is the area of the cross-section, I_x and I_y are the inertia moments, and J is the torsion constant. Other parameters are defined as

$$\begin{cases} A_{\mathrm{eq}} = \int_A \mathrm{d}A + \dfrac{\gamma_1}{\gamma_{\mathrm{s}}}\int_{A_1}\mathrm{d}A_1, \\ G_{x_1} = \int_{A_1} y\mathrm{d}A_1,\ G_{y_1} = \int_{A_1} x\mathrm{d}A_1, \\ I_{x_1} = \int_{A_1} y^2\mathrm{d}A_1,\ I_{y_1} = \int_{A_1} x^2\mathrm{d}A_1, \\ H_u = A_{\mathrm{eq}}y_{\mathrm{s}} - \dfrac{\gamma_1}{\gamma_{\mathrm{s}}}G_{x_1},\ H_v = -\dfrac{\gamma_1}{\gamma_{\mathrm{s}}}G_{y_1}, \\ I_p = I_x + I_y + \dfrac{\gamma_1}{\gamma_{\mathrm{s}}}(I_{x_1} + I_{y_1}) - \dfrac{2\gamma_1}{\gamma_{\mathrm{s}}}G_{x_1}y_{\mathrm{s}} + A_{\mathrm{eq}}y_{\mathrm{s}}^2, \end{cases} \tag{13}$$

where $\int_A \mathrm{d}A$ and $\int_{A_1} \mathrm{d}A_1$ are the area integrations of the cross-sections of the girder and the accessory members, respectively.

With the introduction of the shape functions, the displacement of the element can be expressed by virtue of the nodal displacement vectors as

$$\begin{cases} w_{\mathrm{G}} = \boldsymbol{N}_w \boldsymbol{W}, \\ u_{\mathrm{s}} = \boldsymbol{N}\boldsymbol{U}, \\ v_{\mathrm{s}} = \boldsymbol{N}\boldsymbol{V}, \\ \theta = \boldsymbol{N}_w \boldsymbol{\Theta}, \end{cases} \tag{14}$$

where the shape functions are

$$\begin{cases} \boldsymbol{N}_w = \left\{1-\dfrac{z}{L_{ij}}, \dfrac{z}{L_{ij}}\right\}, \\ \boldsymbol{N} = \left\{1-3\left(\dfrac{z}{L_{ij}}\right)^2+2\left(\dfrac{z}{L_{ij}}\right)^3, \quad z-2\dfrac{z^2}{L_{ij}}+\dfrac{z^3}{L_{ij}^2}, \right. \\ \qquad \left. 3\left(\dfrac{z}{L_{ij}}\right)^2-2\left(\dfrac{z}{L_{ij}}\right)^3, \quad -\dfrac{z^2}{L_{ij}}+\dfrac{z^3}{L_{ij}^2}\right\}, \end{cases} \tag{15}$$

where L_{ij} is the length of the element. The nodal displacement vectors of the element are

$$\begin{cases} \boldsymbol{W} = \left\{w_i \quad w_j\right\}^{\mathrm{T}}, \\ \boldsymbol{U} = \left\{u_i \quad u_i' \quad u_j \quad u_j'\right\}^{\mathrm{T}}, \\ \boldsymbol{V} = \left\{v_i \quad v_i' \quad v_j \quad v_j'\right\}^{\mathrm{T}}, \\ \boldsymbol{\Theta} = \left\{\theta_{zi} \quad \theta_{zj}\right\}^{\mathrm{T}}, \end{cases} \tag{16}$$

where the subscripts i and j represent the parameters of the two nodes of the element. The equation of motion of the beam element considering the effect of the mass of the accessory members can be obtained by introducing Eq. (13) into Eq. (11).

2.2 Equation of motion for the vehicle-bridge interaction

In the computation of the vehicle-bridge interaction, the equation of motion of the bridge is

$$\boldsymbol{M}\ddot{\boldsymbol{u}} + \boldsymbol{C}\dot{\boldsymbol{u}} + \boldsymbol{K}\boldsymbol{u} = \boldsymbol{F}(t), \tag{17}$$

where $\boldsymbol{M}$ is the mass matrix, $\boldsymbol{K}$ is the stiffness matrix, $\boldsymbol{C}$ is the damping matrix of the structure, $\ddot{\boldsymbol{u}}$, $\dot{\boldsymbol{u}}$ and $\boldsymbol{u}$ are the acceleration, velocity, and displacement responses, respectively, of the bridge, and $\boldsymbol{F}(t)$ is the external force vector of the bridge. The Rayleigh damping

$$\boldsymbol{C} = \alpha_0 \boldsymbol{M} + \beta_0 \boldsymbol{K} \tag{18}$$

is adopted, where α_0 and β_0 are the Rayleigh damping factors.

The mass-spring-damping system (Fig. 4) is adopted to simulate the vehicle (Task Committee on Bridge Vibration, JSCE, 1993). 4-DOF is considered: the vertical displacement, the rotation of the vehicle body, and the vertical displacements of the two wheel axles.

The equation of motion of the vehicle model is

$$\boldsymbol{M}_{\mathrm{c}}\ddot{\boldsymbol{u}}_{\mathrm{c}} + \boldsymbol{C}_{\mathrm{c}}\dot{\boldsymbol{u}}_{\mathrm{c}} + \boldsymbol{K}_{\mathrm{c}}\boldsymbol{u}_{\mathrm{c}} = \boldsymbol{F}_{\mathrm{c}}(t), \tag{19}$$

where $\boldsymbol{M}_{\mathrm{c}}$, $\boldsymbol{K}_{\mathrm{c}}$, and $\boldsymbol{C}_{\mathrm{c}}$ are the mass, stiffness and damping matrices respectively, of the vehicle model, $\boldsymbol{F}_{\mathrm{c}}(t)$ is the vehicular load vector, $\ddot{\boldsymbol{u}}_{\mathrm{c}}$, $\dot{\boldsymbol{u}}_{\mathrm{c}}$ and $\boldsymbol{u}_{\mathrm{c}}$=[$\theta$, z_{s}, z_{TF}, z_{TR}]$^{\mathrm{T}}$ are the acceleration, velocity and displacement vectors respectively, with θ denoting the rotation of the vehicle body, and z_{s}, z_{TF}, and z_{TR} are the vertical displacements of the vehicle body, front wheel, and rear wheel, respectively.

The interaction force between the bridge and the vehicle can be expressed as

$$\begin{cases} F_{\mathrm{F}} = -\left(m_{\mathrm{SF}}\ddot{z}_{\mathrm{s}} + m_{\mathrm{TF}}\ddot{z}_{\mathrm{TF}}\right) + \left(m_{\mathrm{SF}} + m_{\mathrm{TF}}\right)g, \\ F_{\mathrm{R}} = -\left(m_{\mathrm{SR}}\ddot{z}_{\mathrm{s}} + m_{\mathrm{TR}}\ddot{z}_{\mathrm{TR}}\right) + \left(m_{\mathrm{SR}} + m_{\mathrm{TR}}\right)g, \end{cases} \tag{20}$$

where

$$\begin{cases} m_{\mathrm{SF}} = \dfrac{M_{\mathrm{s}}\lambda_{\mathrm{R}}^2 + J_{\mathrm{s}}}{\lambda^2}, \\ m_{\mathrm{SR}} = \dfrac{M_{\mathrm{s}}\lambda_{\mathrm{F}}^2 + J_{\mathrm{s}}}{\lambda^2}, \end{cases} \tag{21}$$

where M_{s} and J_{s} are the mass and inertia mass respectively, of the vehicle body, λ is the distance between the two wheels, m is the mass of the wheels. The subscripts F and R indicate the front and the rear wheels, respectively.

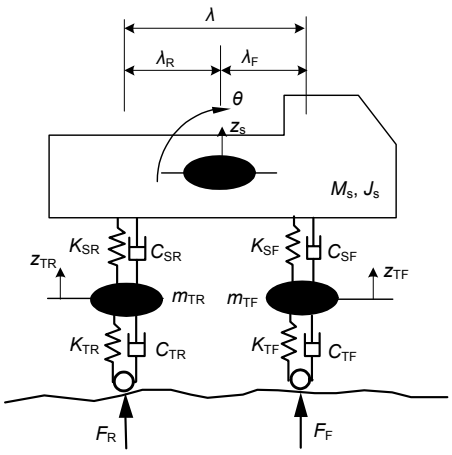

Fig. 4 4-DOF model of vehicle

Eqs. (17) and (19) should be calculated through iterations because of the vehicle-bridge interaction. The Newmark-β method is adopted, and the convergence of the iteration depends on the values of the interaction forces F_F and F_R.

3 Computation model of a CSB

3.1 Parameters of the bridge and vehicles

The Northern Channel Bridge of Hangzhou Bay in Ningbo, China, was taken as a case study to investigate the effect of the local vibration of cables on responses of long-span CSBs to vehicular loads. Fig. 5 shows the design scheme of the bridge, a CSB, with a center span of 448 m and two side spans each of 230 m, with steel box girder. The three piers of the half of the bridge are noted as P1, P2 and P3, respectively. The middle pier P2 is located in the side span, 70 m away from the end of the girder. The displacement of the girder in the longitudinal direction is independent of that of the tower. Detailed information on the parameters of the structures is listed in Table 1. Each cable is divided into ten interlinking elements, and the first four orders of modes are considered in dynamic analysis.

The Rayleigh damping factors were α=0.05 and β=0.0005. Fig. 6 shows the distribution of the damping ratio with respect to the frequency f, which is lower than 1% in the range of the primary frequencies of the bridge. The parameters of a vehicle weighing 250 kN are listed in Table 2.

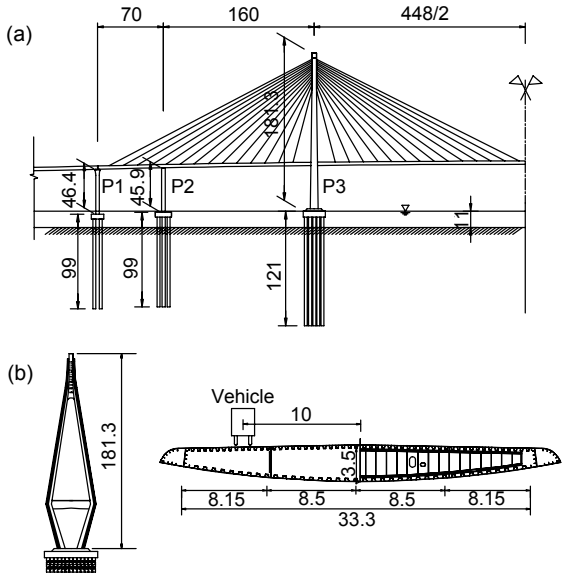

Fig. 5 Scheme of the Northern Channel Bridge of Hangzhou Bay in Ningbo, China (unit: m)
(a) Side view of the bridges; (b) Front view of the tower and cross-section of the girder

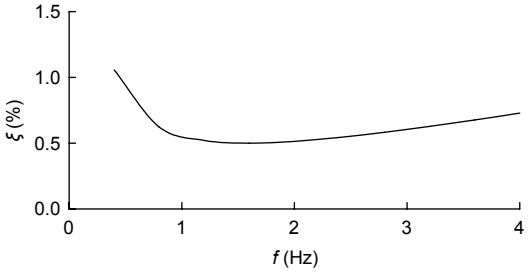

Fig. 6 Distribution of damping ratio

Table 2 Vehicle parameters

Parameter	Value	Parameter	Value
M_s ($\times10^3$ kg)	23.0	m_{TR} ($\times10^3$ kg)	1.6
J_s ($\times10^3$ kg·m^2)	86.25	K_{TF} (kN/m)	2400
K_{SF} (kN/m)	1200	K_{TR} (kN/m)	9600
K_{SR} (kN/m)	4800	C_{TF} (kN·s/m)	6.0
C_{SF} (kN·s/m)	5.0	C_{TR} (kN·s/m)	24.0
C_{SR} (kN·s/m)	20.0	λ_F (m)	2.5
m_{TF} ($\times10^3$ kg)	0.4	λ_R (m)	1.5

Table 1 Sectional characteristics of the Northern Channel Bridge of Hangzhou Bay in Ningbo, China

Structure component	Area (m^2)	Bending stiffness (m^4)		Torsional stiffness	Warping stiffness
		I_x	I_y	J (m^4)	I_w (m^4)
Girder	1.452	2.597	154.070	7.0443	127.480
Tower	11.975–57.515	21.035–223.910	33.636–556.542	26.619–475.470	–
Cable	0.00419–0.00857	–	–	–	–

3.2 Numerical simulation of the road surface roughness

The roughness of the road surface is obtained via a stochastic process using the PSD function. The PSDs used in this study are depicted with dashed lines in Fig. 7a, where Ω is the frequency (cycle/m), and $S(\Omega)$ is the DOF of the roughness of the road. Two kinds of roughness (Roughness 1 and 2) were considered, and corresponding PSD curves are presented in Fig. 7a. Both roughness conditions are found in the "A Class" range (very good road surface condition) according to the ISO-8608 (1995). The PSD of Roughness 2 is 10 times that of Roughness 1. By virtue of the PSD, the roughness samples in Fig. 7b were obtained using the Monte Carlo method.

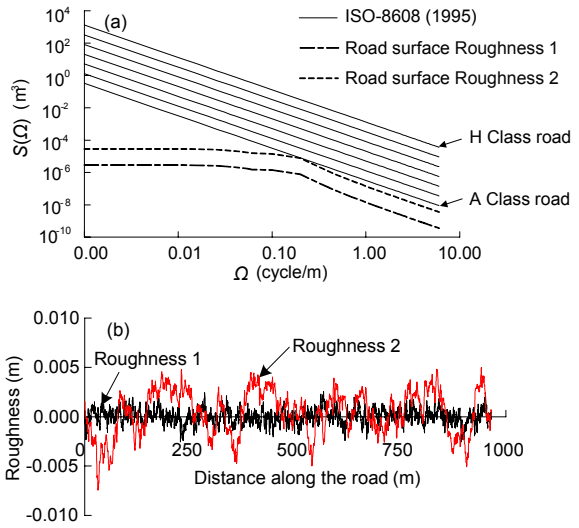

Fig. 7 (a) Power spectral density curve of Roughness 1 and 2; (b) Sample waves of road surface roughness

4 Results and analysis

4.1 Dynamic characteristics of the bridge

Cables were numbered as follows (Fig. 8). The cables in the side span were numbered C_1 to C_{14} from the end of the girder to the tower, and those in the center span were numbered C_{15} to C_{28} from the tower to the span center. Responses of sections A, B and C and the tower top D to vehicle loads were investigated. The cables anchored in sections A, B and C were C_{10}, C_{21} and C_{28}, respectively.

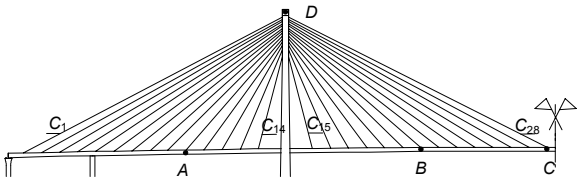

Fig. 8 Cable numbering and the location of the response output

The first two orders of the in- and out-of-plane frequencies of the cables and the frequencies of the global modes of the bridge are shown in Fig. 9. The frequencies of the bridges are close to those of the cables except for the longitudinal floating mode of the bridge, indicating that the vibration of the bridge will easily stimulate the local vibrations of the cables. The primary global modes of the bridge are depicted in Fig. 10, in which the local modes of the cables are also shown.

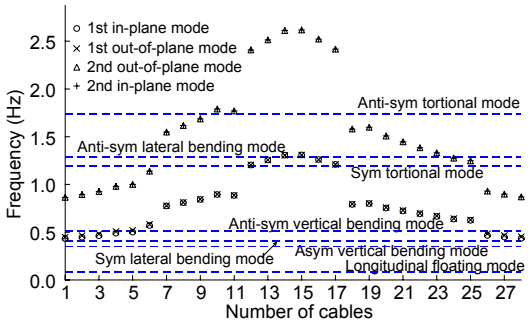

Fig. 9 Frequency range of cables of half of the bridge

The local modes of long cables are observed in global bending modes of the bridge (Fig. 10). The local modes of mid-length cables exist in the second order of anti-symmetry bending mode of the bridge, and the torsion mode of the bridge excites in the local mode of long cables in the span center. The cable-bridge coupling vibrations (Fig. 10) are identical with the distribution of frequencies in Fig. 9.

4.2 Interaction force between the bridge and the vehicle

The vehicle is assumed to travel 10 m from the center line of the bridge (Fig. 5) with a velocity of 20 m/s.

The values of the interaction force F between the wheel axles and the bridge in three road surface roughness conditions are depicted in Fig. 11. $L=v\cdot t$ is the location of the wheels for the vehicle traveling on the bridge, where v is the velocity of the vehicle and t is the traveling time of the vehicle.

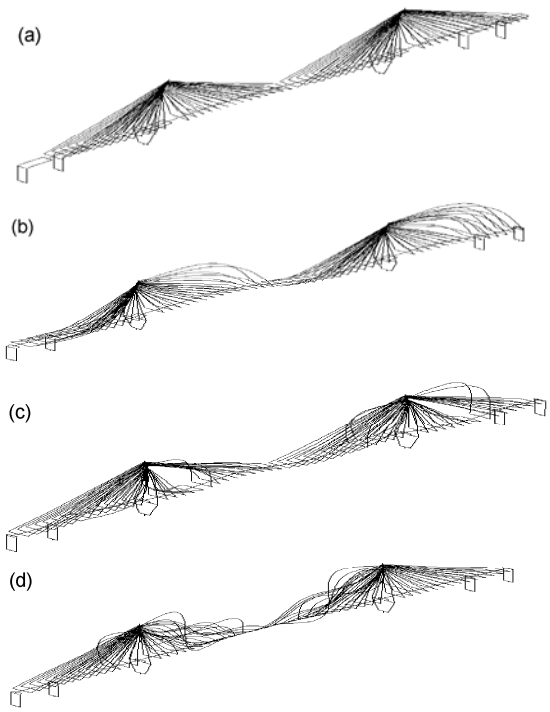

Fig. 10 Primary global modes of cable-stayed bridge
(a) Longtitudinal floating mode 0.08836 Hz; (b) Anti-symmertric vertical bending 0.3981998 Hz; (c) Anti-symmetric vertical bending 0.7858240 Hz; (d) Symmertic torsion 1.198898 Hz

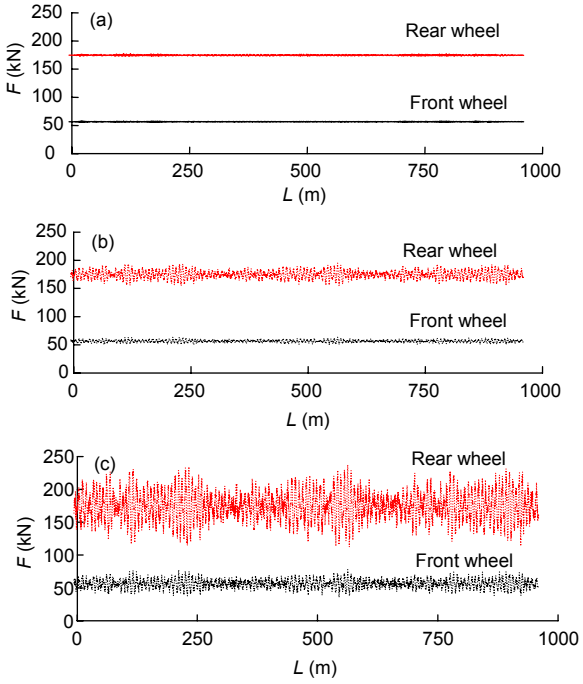

Fig. 11 Vehicular load
(a) Smooth road; (b) Road with Roughness 1; (c) Road with Roughness 2

The roughness of the road surface significantly affects the value of F, especially for the rear wheel under road surface Roughness 2. The interaction force is almost a constant when the road is smooth. Hence, making the road smooth is an effective way to decrease the interaction force between the bridge and vehicles.

4.3 Vibration of the girder

Fig. 12 shows the static and dynamic deflections (u_y) of the girder due to a moving vehicle with a velocity of 80 km/h. When a single vehicle passes through the deck, the vibration amplitude of the tower and the girder is not great and the displacement response is composed mainly of the static deflection. Although the amplitudes of the girder and the tower increase with increasing road surface roughness, the impact factors of the girder and the tower are still very small and the deflections are mainly static ones. Therefore, the impact factors of girders and towers can be valued lower in CSB design.

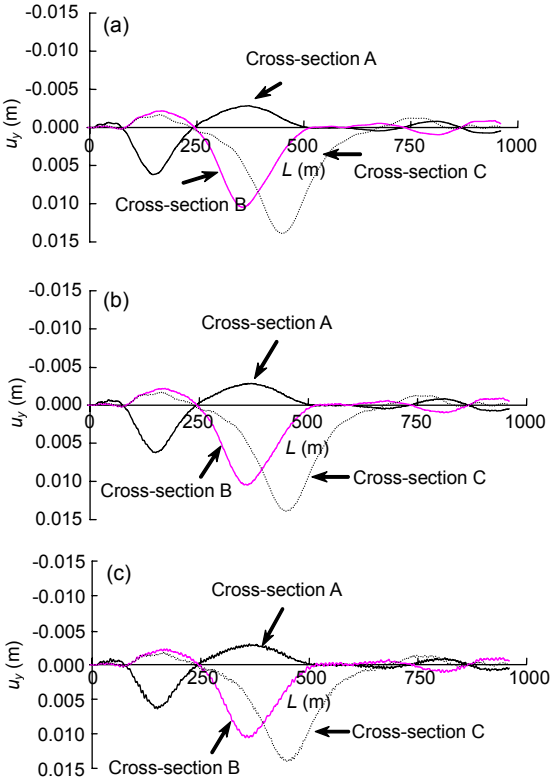

Fig. 12 Displacement responses of the girder
(a) Static deflections; (b) Dynamic displacements when the road is smooth; (c) Dynamic displacements with road Roughness 2

4.4 Vibration of cables

Fig. 13 shows the horizontal and vertical displacement responses in the mid-span of cables of different lengths when the road surface condition is Roughness 2. Compared with that of the girder, the results show that the vibration amplitudes and impact factors of cables due to vehicular loading are greater. For a short cable such as C_{14}, the amplitude of the vibration component in the longitudinal direction of the bridge seems great (Fig. 13a). For a mid-length cable such as C_7, the vertical vibration component caused by the cable-girder interaction is relatively large (Fig. 13b). The value of the vibration amplitude of the long cable C_1 is related to the location of the vehicle. According to the results in Figs. 12 and 13, the effect of the local vibration of cables on the global vibration of the bridge is negligible, although the impact factors of cables are great.

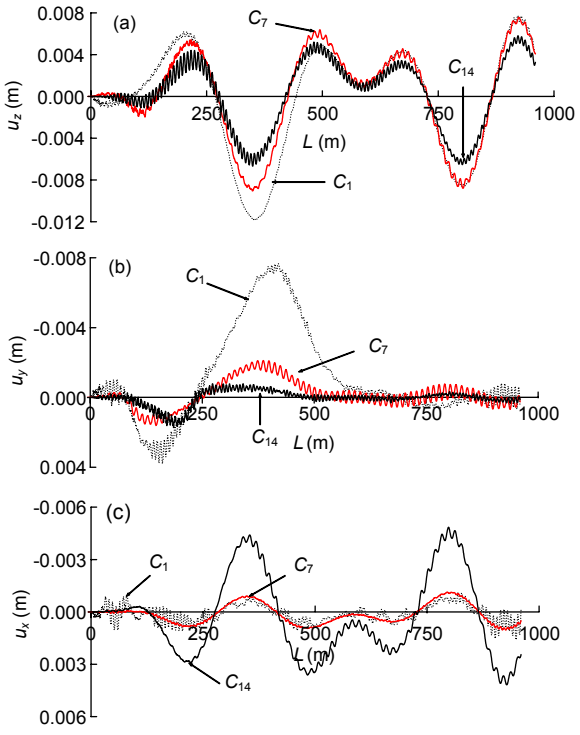

Fig. 13 (a) Horizontal vibration in longitudinal direction, (b) vertical vibration and (c) lateral vibration in transverse direction of cables C_1, C_7 and C_{14}

To investigate the relationship between the local vibration of cables and the global vibration of the bridge, the dynamic responses of cables C_{10}, C_{21} and C_{28} and those of their supports on girders and towers under the road surface condition of Roughness 2 were calculated (Figs. 14–16). The displacement, velocity, and acceleration responses of the tower top were considered as the excitements in the upper supports of C_{10}, C_{21} and C_{28}.

Fig. 14 shows the time histories of the vibrations of cables and their supports in a longitudinal direction. When a vehicle passes the location of the anchorage of the cable, the vibration amplitude of the cable becomes greater than that of the supports on the tower and the girder. When the vehicle moves away from the anchorage of the cable, the displacements of these sections are greater than that of the girder and smaller than that of the tower.

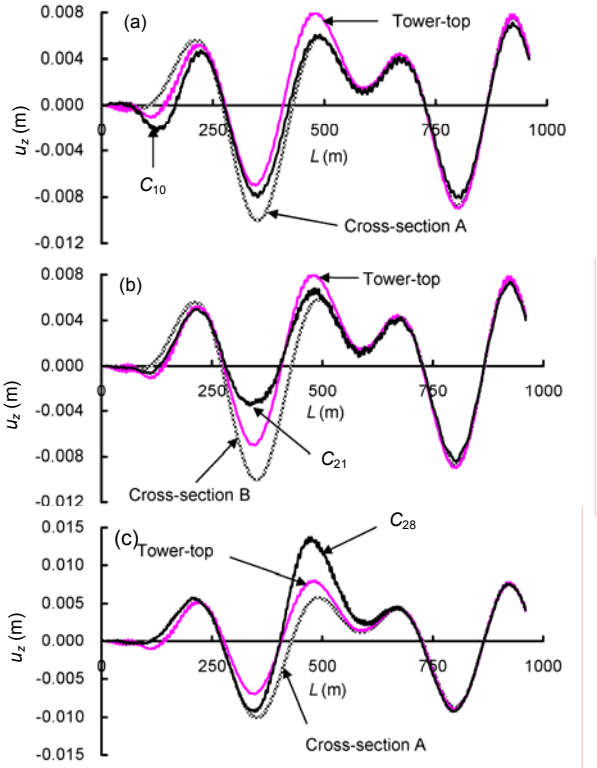

Fig. 14 Time histories of the vibrations of cables and their supports in the longitudinal direction
(a) Cable C_{10}; (b) Cable C_{21}; (c) Cable C_{28}

The vertical displacement responses of cables are depicted in Fig. 15. The displacement responses of C_{10} and C_{21} are greater than those of their supports in towers and smaller than the vibrations of girders. The deflections of the two medium-length cables follow the global displacement responses of girders. However, the vibration of C_{28} is not isochronous with that of its supports, which indicates the occurrence of local vibration of a long-length cable due to a vehicular load.

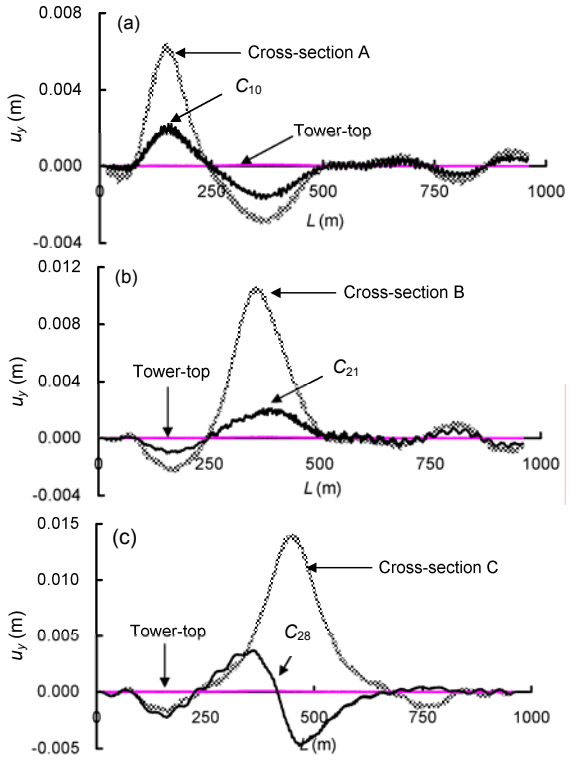

Fig. 15 Time histories of the vibrations of cables and their supports in the vertical direction
(a) Cable C_{10}; (b) Cable C_{21}; (c) Cable C_{28}

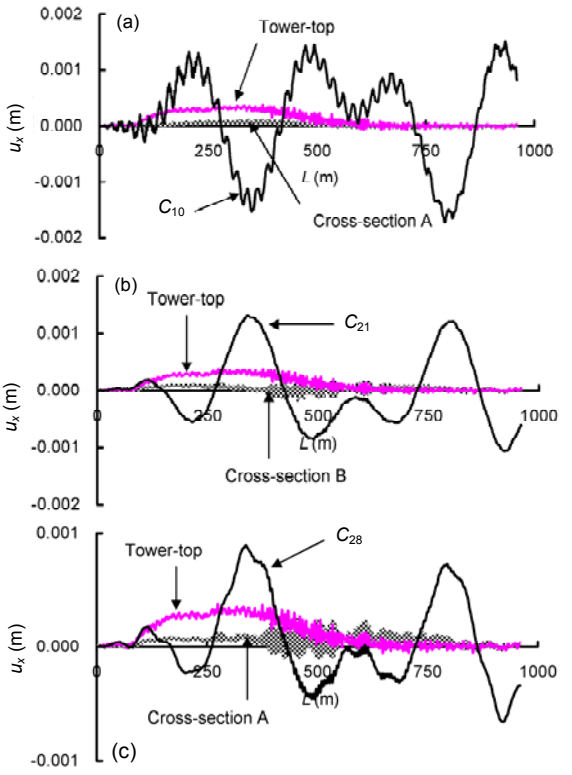

Fig. 16 Lateral vibration of cables and their supports
(a) Cable C_{10}; (b) Cable C_{21}; (c) Cable C_{28}

Lateral vibrations of cables (Fig. 16) are independent of the vibration of their supports on the tower and the girder. The higher frequency component of the lateral vibration of cable C_{10} is the local vibration of the cable.

To investigate the frequency components of a cable's vibrations, the static displacement is subtracted from the dynamic response of the cables and the frequency-domain information is obtained through fast Fourier transform (FFT). The results are depicted in Fig. 17. Most of the prominent components in the vibration of cables are induced by the longitudinal floating mode of the girder, except those of cable C_{28}. The vibrations of C_{28} in vertical view are mainly the cable's local vibration because the anchorage of the cable on the girder is located in the span center which has no deformation in the longitudinal floating mode of the bridge. This indicates that the vibrations of cables are induced mainly by the vibration of their supports.

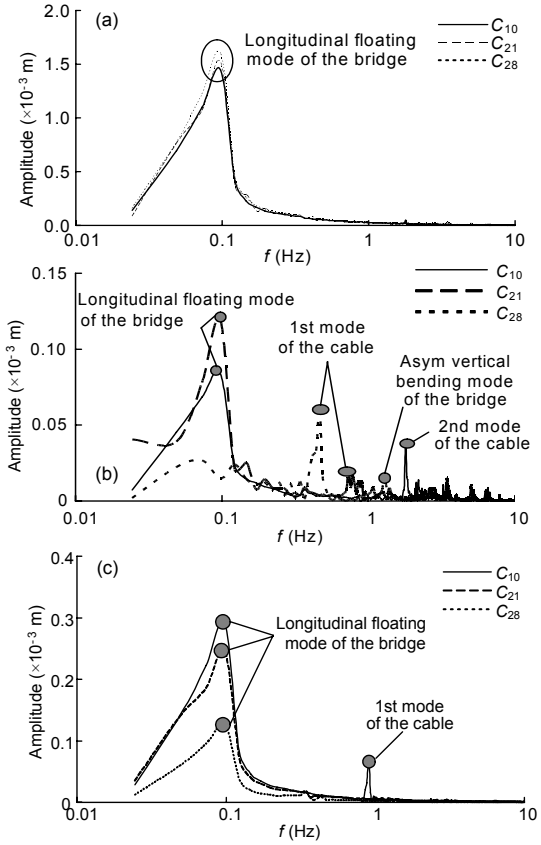

Fig. 17 Amplitude spectra of dynamic displacements of cables C_{10}, C_{21} and C_{28} in the mid-span
(a) In the longitudinal direction; (b) In the vertical direction; (c) In the lateral direction

4.5 Tensions of cables

Fig. 18 shows the time histories of tensions of three cables anchored in the mid-span and three anchored in the side span of the bridge, with a road surface condition of Roughness 2. Compared with the vibration of girders, the variation of cable tensions are greater. The corresponding impact factor of cable tension is about 0.1, which is obviously greater than that of girders and towers. Hence, compared with girders and towers, a higher safety factor should be adopted for cables in the design of CSBs.

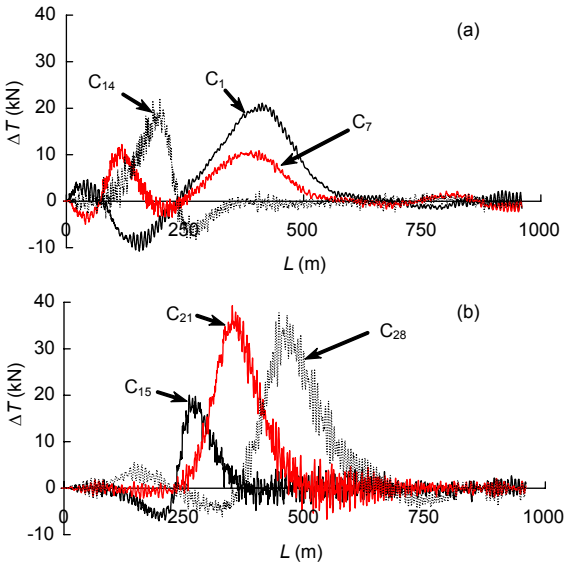

Fig. 18 Tension curves of cables
(a) Cables in side span; (b) Cables in mid-span

5 Conclusions

The dynamic response of a CSB due to vehicular loads was investigated in this paper with consideration of the cables' local vibrations. The Northern Channel Bridge of Hangzhou Bay Bridge, with a center span of 448 m was studied as a case to investigate the dynamic responses of CSBs. We can conclude from the analyses that:

1. Road surface roughness affects the impact value of vehicle loads significantly. The impact value of vehicle loads increases with the road surface roughness.

2. Different structural components show different dynamic responses to the action of vehicular loading. The impact factors of the cable tensions are obviously greater than those of the displacements of girders and towers.

3. The lateral vibrations of cables are independent of the vibration of their supports on the tower and the girder.

4. The vibrations of the cables excited by their supports are greater than those of girders only if a vehicle travels close to the anchorage of the cables.

References

Abdel-Ghaffar, A.M., Khalifa, M.A., 1991. Importance of cable vibration in dynamics of cable-stayed bridges. *ASCE Journal of Engineering Mechanics*, **117**(11):2571-2589. [doi:10.1061/(ASCE)0733-9399(1991)117:11(2571)]

Au, F.T.K., Cheng, Y.S., Cheung, Y.K., 2001. Effects of random road surface roughness and long-term deflection of pre-stressed concrete girder and cable-stayed bridges on impact due to moving vehicles. *Computers and Structures*, **79**(8):853-872. [doi:10.1016/S0045-7949(00)0180-2]

Au, F.T.K., Lou, P., Li, J., Jiang, R.L., Leung, C.C.Y., Lee, P.K.K., Wong, K.Y., Chan, H.Y., 2009. Simulation of Vibrations of Ting-Kau Bridge due to Vehicular Loading. Proceeding of 4th International Symposium on Environment Vibrations–Prediction, Monitoring, Mitigation and Evaluation, Beijing, China, p.1109-1116.

Bruno, D., Greco, F., Lonetti, P., 2008. Dynamic impact analysis of long span cable-stayed bridges under moving loads. *Engineering Structures*, **30**(4):1160-1177. [doi:10.1016/j.engstruct.2007.07.001]

Caetano, E., Cunha, A., Taylor, C.A., 2000. Investigation of dynamic cable-deck interaction in a physical model of a cable-stayed bridge, Part I: modal analysis. *Earthquake Engineering and Structural Dynamics*, **29**(4):481-498.

Caetano, E., Cunha, A, Gattulli, V., Lepidi, M., 2008. Cable-deck dynamic interactions at the International Guadiana Bridge: on-site measurements and finite element modeling. *Structural Control and Health Monitoring*, **15**(3):237-264. [doi:10.1002/stc.241]

Calcada, R., Cunha, A., Delgado, R., 2005a. Analysis of traffic-induced vibrations in a cable-stayed bridge. Part I: Experimental assessment. *ASCE Journal of Bridge Engineering*, **10**(4):370-385. [doi:10.1061/(ASCE)1084-0702(2005)10:4(370)]

Calcada, R., Cunha, A., Delgado, R., 2005b. Analysis of traffic-induced vibrations in a cable-stayed bridge. Part II: Numerical modeling and stochastic simulation. *ASCE Journal of Bridge Engineering*, **10**(4):386-397. [doi:10.1061/(ASCE)1084-0702(2005)10:4(386)]

Das, A., Dutta, A., Talukdar, S., 2004. Efficient dynamic analysis of cable-stayed bridges under vehicular movement using space and time adaptivity. *Finite Elements in Analysis and Design*, **40**(4):407-424. [doi:10.1016/S0168-874X(03)00070-2]

Fujino, Y., Warnitchai, P., Pacheco, B.M., 1993. An experimental and analytical study of autoparametric resonance in a 3DOF model of cable-stayed-beam. *Nonlinear*

Dynamics, **4**:111-138.

Gattulli, V., Lepidi, M., 2007. Localization and veering in cable-stayed bridge dynamics. *Computer and Structures*, **85**(21-22):1661-1668. [doi:10.1016/j.compstruc.2007.02.016]

Guo, W.H., Xu, Y.L., 2001. Fully computerized approach to study cable-stayed bridge-vehicle interaction. *Journal of Sound and Vibration*, **248**(4):745-761. [doi:10.1006/jsvi.2001.3828]

ISO-8608, 1995. Mechanical Vibration-Road Surface Profiles Reporting of Measured Data. International Organization for Standardization (ISO).

Nagai, M., Nii, J., Kawabata, O., 1993. Three Dimensional Dynamic Analysis of Cable-Stayed Bridges Including Cable Local Vibration. Proceeding of 4th East Asia-Pacific Conference on Structural Engineering & Construction, Seoul, Korea, p.1845-1850.

Task Committee on Bridge Vibration, JSCE, 1993. Measurement and Evaluation of Bridges Vibration. Gihodo Shuppan, Tokyo (in Japanese).

Warnitchai, P., Fujino, Y., Susumpow, T., 1995. A non-linear dynamic model for cables and its application to a cable-structure system. *Journal of Sound and Vibration*, **187**(4):695-712. [doi:10.1006/jsvi.1995.0553]

Wu, Q., Takahashi, K., Okabayashi, T., Nakamura, S., 2003. Response characteristics of local vibrations in stay cables on an existing cable-stayed bridge. *Journal of Sound and Vibration*, **261**(3):403-420. [doi:10.1016/S0022-460X(02)01088-X]

Zaman, M., Taheri, M.R., Khanna, A., 1996. Dynamic response of cable-stayed bridges due to moving vehicles using the structural impedance method. *Applied Mathematical Modelling*, **20**(12):877-889. [doi:10.1016/S0307-904X(96)00094-7]

2010 JCR of Thomson Reuters for *JZUS-A* and *JZUS-B*

ISI Web of Knowledge℠

Journal Citation Reports®

WELCOME HELP RETURN TO LIST

2010 JCR Science Edition

Journal: Journal of Zhejiang University-SCIENCE A

Mark	Journal Title	ISSN	Total Cites	Impact Factor	5-Year Impact Factor	Immediacy Index	Citable Items	Cited Half-life	Citing Half-life
☐	J ZHEJIANG UNIV-SC A	1673-565X	442	0.322		0.050	120	3.7	7.1

Journal: Journal of Zhejiang University-SCIENCE B

Mark	Journal Title	ISSN	Total Cites	Impact Factor	5-Year Impact Factor	Immediacy Index	Citable Items	Cited Half-life	Citing Half-life
☐	J ZHEJIANG UNIV-SC B	1673-1581	770	1.027		0.137	124	3.5	7.5